Geophysical Prospecting EAGE EUROPEAN ASSOCIATION OF GEOSCIENTISTS & ENGINEERS

Geophysical Prospecting, 2013, **61**, 857–873 doi: 10.1111/1365-2478.12024

Fast mapping of magnetic basement depth, structure and nature using aeromagnetic and gravity data: combined methods and their application in the Paris Basin

G. Martelet*, J. Perrin, C. Truffert and J. Deparis

BRGM, ISTO, UMR 7327, 45060 Orléans, France

Received July 2011, revision accepted November 2012

ABSTRACT

Assessment of deep buried basin/basement relationships using geophysical data is a challenge for the energy and mining industries as well as for geothermal or CO_2 storage purposes. In deep environments, few methods can provide geological information; magnetic and gravity data remain among the most informative and cost-effective methods. Here, in order to derive fast first-order information on the basement/basin interface, we propose a combination of existing and original approaches devoted to potential field data analysis. Namely, we investigate the geometry (i.e., depth and structure) and the nature of a deep buried basement through a case study SW of the Paris Basin. Joint processing of new high-resolution magnetic data and up-to-date gravity data provides an updated overview of the deep basin.

First, the main structures of the magnetic basement are highlighted using Euler deconvolution and are interpreted in a structural sketch map. The new high-resolution aeromagnetic map actually offers a continuous view of regional basement structures and reveals poorly known and complex deformation at the junction between major domains of the Variscan collision belt.

Second, Werner deconvolution and an ad hoc post-processing analysis allow the extraction of a set of magnetic sources at (or close to) the basin/basement interface. Interpolation of these sources together with the magnetic structural sketch provides a Werner magnetic basement map displaying realistic 3D patterns and basement depths consistent with data available in deep petroleum boreholes.

The last step of processing was designed as a way to quickly combine gravity and magnetic information and to simply visualize first-order petrophysical patterns of the basement lithology. This is achieved through unsupervised classification of suitably selected gravity and magnetic maps and, as compared to previous work, provides a realistic and updated overview of the cartographic distribution of density/magnetization of basement rocks.

Altogether, the three steps of processing proposed in this paper quickly provide relevant information on a deep buried basement in terms of structure, geometry and nature (through petrophysics). Notwithstanding, limitations of the proposed procedure are raised: in the case of the Paris Basin for instance, this study does not provide proper information on Pre-Mesozoic basins, some of which have been sampled in deep boreholes.

Key words: Aeromagnetic, Gravity, Werner, Euler, Basement, Paris Basin

*E-mail: g.martelet@brgm.fr

INTRODUCTION

Mapping buried basement geometry, as well as its geological nature is of critical importance for several industries, including petroleum and unconventional resource exploration, coal mining and geothermal energy. In thick sedimentary basins where electric/electromagnetic methods or even petroleum seismic data cannot provide information at sufficient depth, potential field methods (i.e., gravity and magnetics) remain the only data capable of providing valuable regional and relatively high- resolution information on the basement.

In the present paper, combining several fast processing methods, we aim at extracting from potential field data relevant information in order to characterize the geometry (i.e., depth and structure) and the nature of the basement below the south-western part of the Paris Basin. This study takes advantage of a recent high-resolution airborne magnetic and radiometric survey conducted by the Bureau de Recherches Géologiques et Minières (BRGM, French geological survey) in 2008–2009 over Région Centre, France (Perrin *et al*. 2009), complemented by available ground gravity data and deep borehole information. An exhaustive integrated geological interpretation, including seismic data, careful interpretation of boreholes and petrophysical measurements is beyond the scope of this article: for this study, we chose to focus on the methodology of analysis of potential field data in order to derive first-order information quickly.

A wealth of methods and algorithms have been developed since the middle of the 20th century to model and interpret gravity and magnetic maps in terms of depth, structure and nature of a basement (e.g., Nabighian *et al*. 2005). They fall into two categories: the first one aims at providing a description of the geology as realistic as possible, by forward or inverse modelling of geological bodies. In order to achieve proper results, these methods require the introduction of as much independent information as possible. In this study, since our available independent information is limited to 41 deep boreholes in an area of approximately 40 000 km^2, we choose to use a second category of methods developed to analyse potential field data; these methods use a simplified description of the sources that cause the anomalies (i.e., sphere, pipe, thin or thick sheets, contact) and they provide results independently of the susceptibility/density contrasts (e.g., Gunn 1997; Li 2003).

To our knowledge, no study has ever been published that derives a basement geometry in the Paris Basin, based on potential field methods. This may be due to a lack of sufficiently high-resolution magnetic data. The new high-resolution aeromagnetic survey of Région Centre should bring new and accurate constraints both on the structure of the basement and its depth and geometry. We tested several processing methods in order to extract such information from the data. We retained a combination of Euler and Werner deconvolutions for structural interpretation and basement depth mapping respectively.

Conversely, several previous studies (e.g., Gérard 1971; Mégnien 1980; Debeglia and Weber 1985; Corpel and Debeglia 1988; Galdeano and Guillon 1988) have attempted to decipher the nature of the Paris Basin basement using gravity and magnetic data. Most of them used the global aeromagnetic survey of France (Le Borgne and Le Mouel 1966) flown at 3000 m altitude, with a line spacing of 10 km, which provided a low-resolution magnetic map. Weber (1973) and Weber and Lorne (1966) addressed the same issue in the extreme south and south-western part of the basin, using even older aeromagnetic surveys but with slightly higher resolution; as did Corpel and Debeglia (1988) in the central part of the basin using a CGG (Compagnie Générale de Géophysique) mid-resolution aeromagnetic survey flown in 1985.

The combination of new high-resolution magnetic data, improved gravity data and the use of original joint processing of these data sets is proposed in order to provide an updated overview of the basin's basement, which is briefly discussed in terms of Pre-Mesozoic tectonics of the basin.

DATA

BRGM conducted a fixed-wing magnetic and gamma spectrometric survey, from August 2008–February 2009, on a large south-western portion of the Paris Basin, over the Région Centre. Covering about 40 000 km^2 along flight-lines oriented N-S and equally spaced at a distance of 1 km, this survey, flown at an average 85 m ground clearance, provides new high-resolution magnetic and radiometric maps at a regional scale. A detailed description of the survey is given in Perrin *et al*. (2009); here we focus on the magnetic data set and its processing in order to derive information on the magnetic basement of the basin. A map of the vertical derivative of the magnetic anomaly reduced to the pole is presented in Fig. 1. This map is preferred to a simple anomaly map because it enhances the structures and magnetic patterns that are addressed in the paper. This choice is further detailed in the following paragraphs as well as comments on the magnetic map.

Gravity data used in this study derive from the compilation of ground gravity surveys conducted in France since the middle of the 20th century and compiled within the Banque Gravimétrique de la France (BGF) (Martelet, Pajot and Debeglia 2009). The station coverage within the study area, on

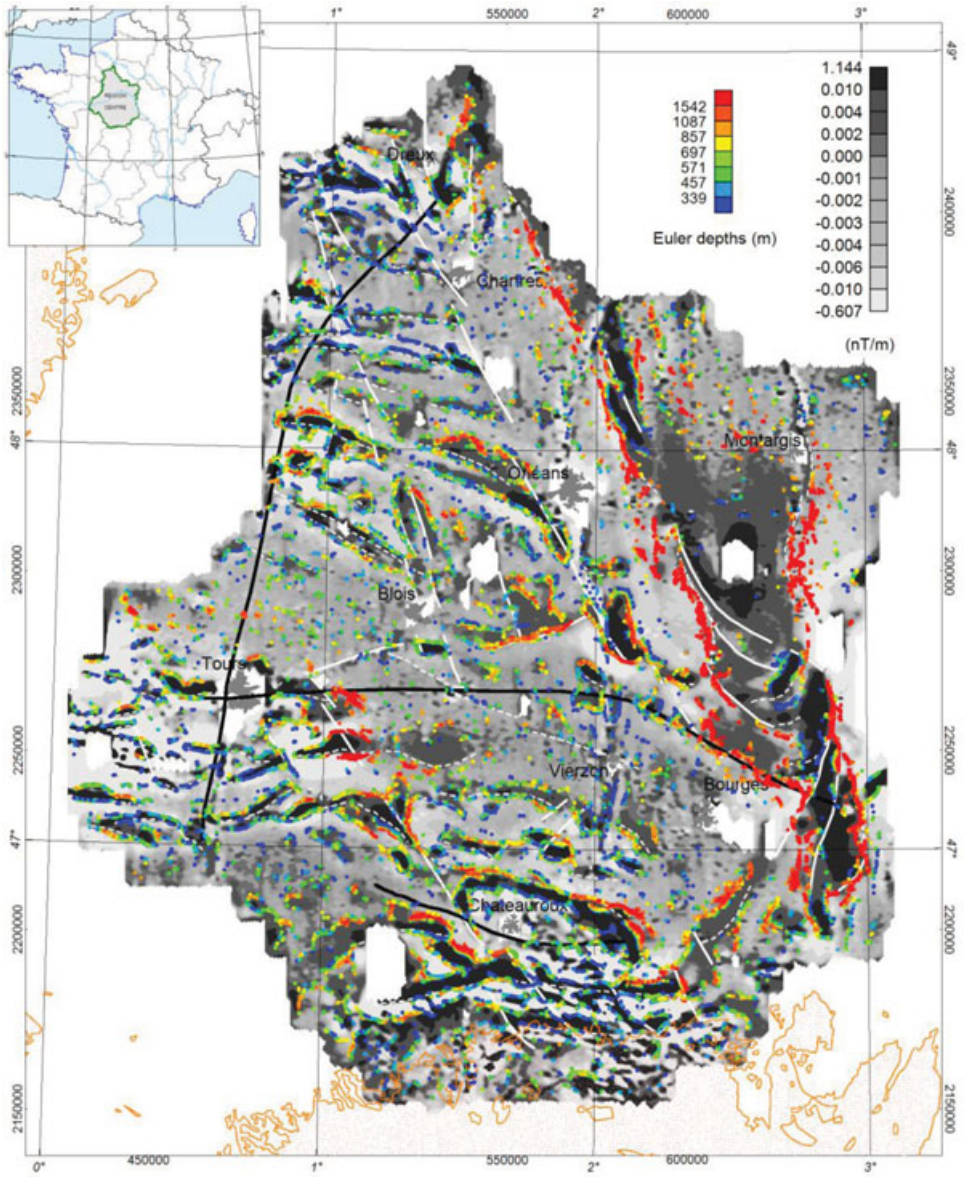

Figure 1 Map of the vertical gradient of the magnetic anomaly reduced to the pole (grey shades) in Région Centre, Paris Basin, France (location in insert); surrounded by an outcropping basement (in orange) of Massif Central to the south and Massif Armoricain to the west. Euler solutions are superimposed as colour-coded dots displaying the main magnetic gradient zones and the depth of their causative sources. Magnetic trends (white dashed lines) were interpreted from the Euler sources and interruption of these trends, interpreted as regional tectonic structures are outlined as white plain lines. Locations of the cross-sections of Figs 6 and 7 are displayed as thick black lines.

average, is about 1 station/km^2 (Fig. 2). Data are tied to the CGF65 base station network; all standard corrections with a reference density of 2600 kg/m^3 and terrain corrections computed to a distance of 167 km (Martelet, Debeglia and Truffert 2002) are included in order to derive the Bouguer anomaly. Taking into account the accuracy of 1) the network, 2) the measurements of gravity and positioning and 3) the terrain corrections, the RMS error on the Bouguer anomaly is 0.32 mGal in the study area. A map of the vertical derivative of the Bouguer anomaly is presented in Fig. 2. This map is preferred to a Bouguer anomaly map because the vertical gradient operator focuses on the anomalies, while removing the regional wavelengths of the field and at the same time attenuating the effect of the sedimentary pile (which is essentially smooth: black thick contours in Fig. 2). This map therefore enhances the density patterns of the basement that are addressed

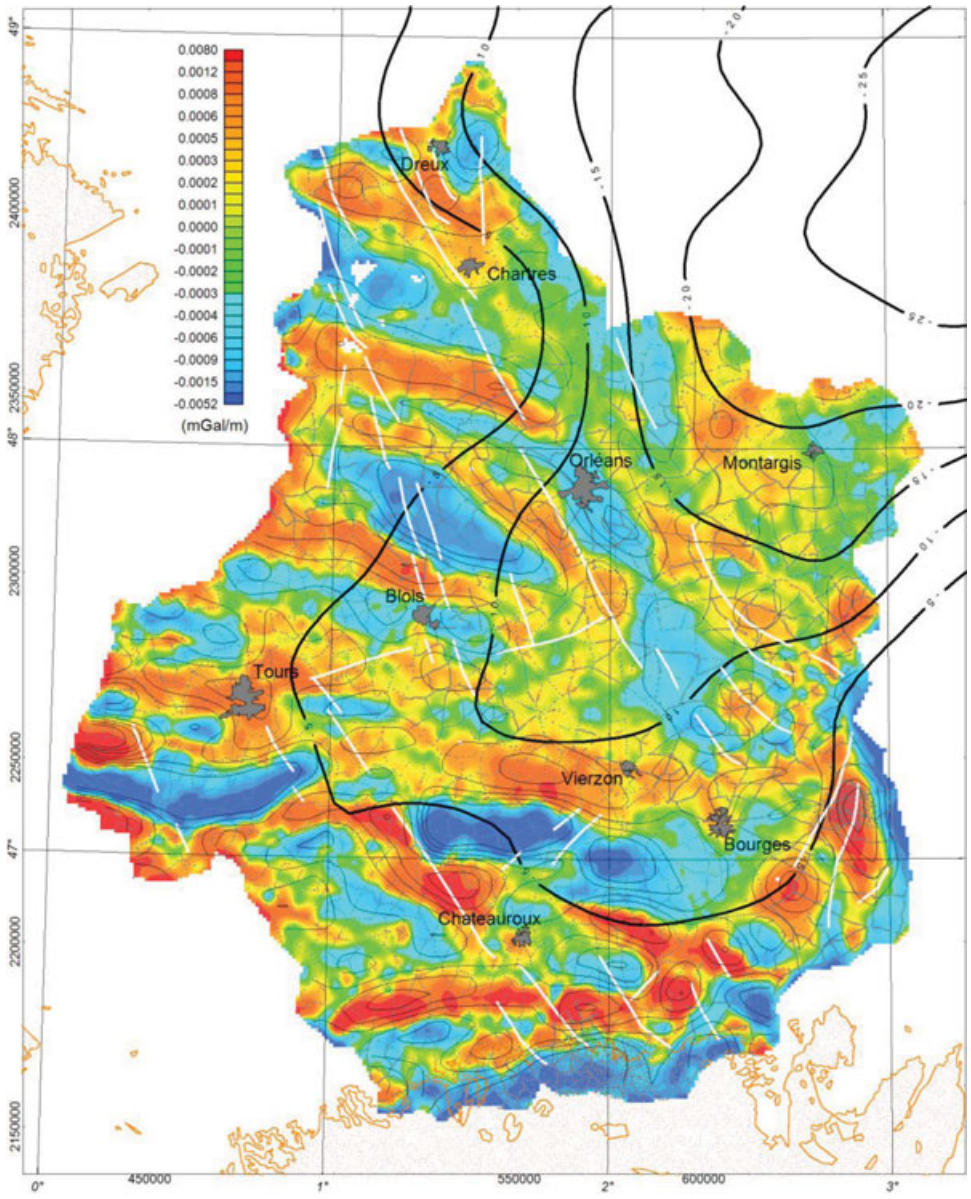

Figure 2 Map of the vertical gradient of the Bouguer anomaly (colour shades) with location of the interpolated gravity data (grey dots). The thick black and thin black contours respectively correspond to the gravity effect of the sedimentary pile and the Bouguer anomaly at the top of the basement, as evaluated by stripping in a previous study (Corpel and Debeglia 1988). See text for comments.

in the paper. This choice is further detailed in the following paragraphs as well as comments on the gravity map.

Other data used to constrain the potential field interpretation include a simplified geological map of the studied region, extracted from the 1:1M scale geological map of France (Chantraine *et al.* 1996) and the depth to the basement derived from 41 scattered deep boreholes. A grid of the basement surface, previously interpolated based on the deep boreholes only (Chantraine *et al.* 1996) is also used as a reference.

DEPTH AND STRUCTURE OF THE MAGNETIC BASEMENT

Methodology

A review of available methods that can be used for the interpretation of potential field data reveals a considerable number of publications on this topic since the middle of the 20th century. These methods essentially fall into two categories: the first one aims at providing a description of the geology that

is as realistic as possible, by forward or inverse modelling of geological bodies.

Inverse methods can be reliable in specific geological contexts where a hypothesis such as two-layer models (e.g., Oldenburg 1974), thin sheet or maximum compactness for instance (e.g., Guillen and Menichetti 1984) can be assumed as a regularization constraint of the inversion process. Stochastic inversion (Bosch, Guillen and Ledru 2001; Guillen *et al*. 2008) can be a very powerful method of providing indicators of the statistical reliability of output inversed models; however, it requires a relatively detailed knowledge of the geology that is input as a starting model. Similarly, forward modelling, which probably allows attaining the most realistic models, requires the introduction of as much independent information as possible to achieve reliable results (e.g., Martelet *et al*. 2004; Talbot *et al*. 2004; Joly *et al*. 2008; Marello, Ebbing and Gernigon 2010).

On the other hand, a second category of methods was developed to analyse potential field data, based on a simplified description of the sources (i.e., sphere, pipes, thin or thick sheets, contacts) that cause the anomalies; these methods are independent of the susceptibility/density contrast (e.g., Gunn 1997; Li 2003). Among those methods, empirical graphical procedures were first proposed (e.g., Peters 1949); the next stage was devoted to comparing the observed field to analytic models, first by means of charts (e.g., de Gery and Naudy 1957) and later through a variety of different techniques that use synthetic model fitting, such as Werner deconvolution (e.g., Werner 1953; Hartman, Teskey and Friedberg 1971; Hansen and Simmonds 1993; Phillips 1997; Hansen 2005), Euler deconvolution (e.g., Thompson 1982; Reid *et al*. 1990) and the analytical signal (e.g., Nabighian 1972; Roest, Verhoef and Pilkington 1992). Extensive applications and improvements of these methods have been published, such as the use of vertical gradients (e.g., Marson and Klingele 1993; Debeglia and Corpel 1997), or taking into account the effect of noise in data (Keating 1998). These techniques assumed a chosen geometry of the source. Progressively, Huang (1996), Stavrev (1997), Ku and Sharp (1983) and Barbosa, Silva and Medeiros (1999) investigated the simultaneous recovery of both shape, depth and/or dip of sources using methods derived from Euler deconvolution by adapting the analytic signal technique of Hsu, Coppens and Shyu (1998). With the same goal, 'extended Euler deconvolution' was proposed by Mushayandebvu *et al*. (1999) and recognized by Nabighian and Hansen (2001) as a unification of Euler and Werner deconvolutions. The same kind of results was achieved using wavelet transforms (Moreau *et al*. 1997; Sailhac *et al*. 2000; Martelet *et al*. 2001; Yang *et al*. 2010).

Rather than using a sophisticated method to simultaneously determine the position, shape, dip and magnetic susceptibility of magnetic sources (because without exterior constraints we would not have been able to properly interpret this information) we chose to proceed in two steps: 1) determining the geometry (i.e., the depth and structure) of the magnetic basement and 2) mapping the magnetization / density contrasts of the basement, which is the last step before interpreting the nature of the basement.

We studied the structure and geometry of the basement using Euler and Werner deconvolutions respectively. Both methods, in their original form, were designed to provide the position (in X, Y and Z) of causatives sources assuming a simplified geometry of the source. Since the user chooses the geometry of the source *a priori*, the associated form of the induced field is analytically known and the deconvolution process thus essentially consists in finding the X, Y and Z of the source that best fits the measured anomaly. Numerically, this is achieved by solving a system of redundant equations within a moving window. This basic principle has been described in several publications and algorithms, either in 2D or 3D, including different refinements in order to filter and/or cluster the computed solutions.

We performed standard Euler deconvolution of the magnetic anomaly grid, as well as Werner deconvolution of the magnetic anomalies along flight lines (Hartman *et al*. 1971; Phillips 1997). We then carefully reviewed the solutions obtained in order to remove as much spurious solutions as possible before further interpretation. In fact, the two numerical deconvolution methods that we applied can provide results largely obscured by the presence of spurious sources; their most frequent origin is noise in the data, interference of adjacent anomalies and unsuitable choice of the deconvolution window with respect to the targets. Also, the presence of intrasedimentary magnetic sources can produce shallow solutions that may lead to misinterpretation when the target is the basement depth. Furthermore, the algorithms we used intrinsically produce clouds of solutions: 1) in Euler deconvolution, because one solution is computed at each position of the moving window and therefore several sources are generally determined for one anomaly; and 2) in Werner deconvolution, for the same reason and also because variable size windows are used. A description of the strategy and parameters adopted to reduce the number of spurious solutions is provided in the next paragraph.

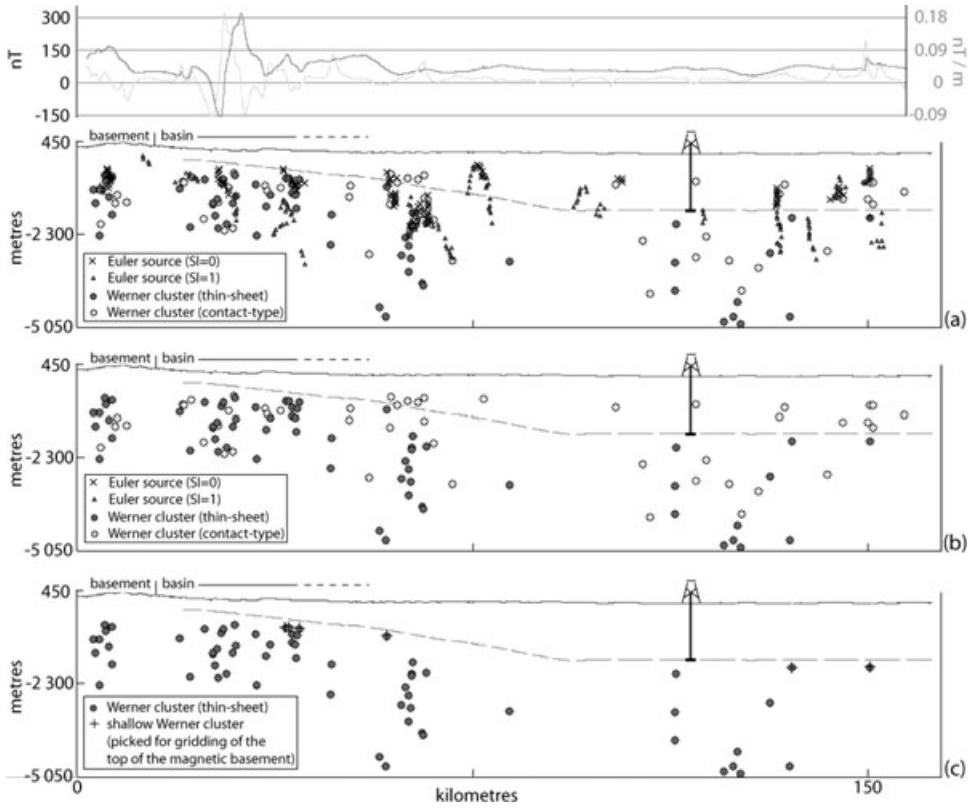

Figure 3 Example of a cross-section along a 150 km long N-S flight-line, ranging from the outcropping basement (left) to the centre of the basin (right), displaying the topography (upper bound of the graphs), a drill hole reaching a previously interpolated basement (dashed line) (Chantraine *et al*. 1996) and magnetic sources: (a) comparison of Euler sources (SI = 0, represented by crosses; SI = 1, represented by triangles) and Werner sources: contact-type and thin-sheet sources (respectively white and grey circles); (b) Werner sources: contact-type and thin-sheet sources (respectively white and grey circles); (c) Werner thin-sheet sources (grey circles) and selection of the most superficial such sources (crosses).

Processing

Processing was divided into three stages in order to derive a realistic geometry of the 3D surface of the magnetic basement: 1) main structures of the magnetic basement were highlighted using Euler deconvolution and interpreted in a structural sketch map, 2) Werner deconvolution and ad hoc post-processing allowed to extract a set of magnetic sources at (or close to) the magnetic basement and 3) these sources, together with the available depth of basement in the boreholes were interpolated taking into account the structures.

We adopted a dual Euler/Werner strategy. Euler solutions, better than Werner solutions, provide detailed cartographic support for structural mapping as well as, in some places, coherent and useful information to interpret the direction of the plunge of structures (Fig. 1). On the other hand, we experienced that Werner deconvolution and clustering provides reliable solutions in terms of depth to the top of magnetic sources (Fig. 3a).

Euler deconvolution

Euler deconvolution was performed in 3D, using Geosoft 6.1 Euler standard deconvolution. It was applied on a 250 m gridded data set. This grid was interpolated using minimum curvature on 1 km spaced flight lines. These data had previously been culturally-edited along the flight lines, numerically in a first stage (e.g., Hassan *et al*. 1998) and manually to remove remaining complex noises. Once gridded, data were reduced to the pole ($D = -0.87^{\circ}E$, $I = 63.06^{\circ}$) and upward continued of half a grid cell in order to minimize the effect of remaining short wavelength noise and to reduce associated shallow spurious sources. Considering that the target is the basement, this smoothing is not penalizing, except possibly at the extreme south of the study area, on the border of the basin; but in this zone, the interpolation of the basement is well constrained, where the basement reaches the surface. After some tests, Euler deconvolution was performed using a window size equal to 20 times the grid spacing (i.e., 5000 m); this value was chosen

sufficiently large to encompass the characteristic anomalies of the magnetic map and not too large to minimize interference between anomalies during the deconvolution. The expected sources were essentially the lateral contrasts of the magnetic properties within the basement and thus the deconvolution was performed for a 'contact-type' source, with a structural index (SI) of 0. Both the rather large deconvolution window and low SI value contributed to limiting the number of solutions. Filtering of the solutions was however necessary to remove some local 'spray' effects. Thresholding was applied: 1) on the range of depths (limited to between 250–5000 m, corresponding to the grid spacing and deconvolution window size respectively, as usually recommended (e.g., Reid *et al.* 1990), 2) on the depth error estimate, which was kept lower than 15% of the source depth, 3) on the distance from the source to the centre of the deconvolution window that was limited to 1000 m, a value close to the standard deviation of this parameter. Resulting Euler solutions are plotted in Fig. 1.

Most Euler sources are located between a few hundred metres below the topography, down to more than 2000 m at depth. Most sources underline the main magnetic gradients and thus display alignments that were traced out and interpreted as 'magnetic trends' (dashed white lines in Fig. 1). These trends are themselves sometimes interrupted; alignments of such interruptions are interpreted as 'magnetic discontinuities' (plain white lines in Fig. 1). Both magnetic trends and discontinuities produce a simplified magnetic structural sketch map that is further described in the following paragraphs, together with gravity/magnetic signatures of the basement.

Depths of Euler solutions are not discussed here; instead, the next paragraph presents and analyses Werner solution depths that, after clustering are less disseminated than Euler solutions and more straightforward to interpret in terms of magnetic basement depth (as suggested in Fig. 3a). However, Euler sources (SI = 1) and Werner clusters (thin-sheet) are consistent and patterns of Euler solutions provide consistent and useful information for preliminary cartographic interpretations. For instance, the deepest sources of the map (Fig. 1) occur mostly along the PBMA (Paris Basin Magnetic Anomaly – trending N-S to N30W, along the eastern border of the map); this is consistent with the recognized deep intra-basement nature of the magnetic source of the PBMA. Indeed, the source expected within the basement around 2.5–4 km (from magnetic modelling e.g., Bayer, Guillen and Rousset 1988; Guillen *et al.* 1990) was not clearly identified in the core of the Sancerre-Couy borehole, which penetrated the basement from 940 m down to 3500 m depths (Lorenz *et al.* 1987).

Along certain magnetic gradients, one can observe some spreading and depth variations of Euler sources (Fig. 1 and also Fig. 3a in a cross-section view); this is inherent to the method and should not be over-interpreted. In some cases however, the pattern of Euler sources can be indicative of the dip of magnetic structures. For instance, south of the map, around Chateauroux (Fig. 1), an E-W elongated oval area is designed by the Euler sources; within the oval, sources are relatively shallow, around 500 m depth, whereas the northern rim of the structure deepens northwards down to 1500–2000 m. The overall pattern suggests a bulge of the basement, limited to the south by a strong E-W elongated magnetic anomaly previously interpreted as granodioritic (Weber 1973) and that outlines the northern limit of the Massif Central basement. Cartographically, the formation of the bulge seems to result from a dextral strike-slip displacement along the N150E magnetic discontinuity that runs from Tours to Chateauroux and that would have been stopped and folded against the Variscan Massif Central basement block (Chantraine *et al.* 1996).

Werner deconvolution

Werner deconvolution was performed using PDEPTH software (Phillips 1997) along the flight lines, on the culturally edited magnetic anomaly reduced to the pole, 125 m upward continued (equivalent to half a grid cell), as with the Euler deconvolution, in order to minimize the effect of remaining short wavelength noises. After some tests, Werner deconvolution was performed using a min./max. window size of 500/10 000 m in 500 m increments and shifted every 1000 m; this returned a large number of solutions but without too many spreading effects. Computations were performed both on the field and its total horizontal derivative in order to extract thin-sheet and contact-type sources respectively (e.g., Hartman *et al.* 1971). Then, statistical clustering of sources was performed in order to restrict the sources to the most significant and reliable magnetic geological contrasts, thus simplifying the interpretation. During clustering, Werner solutions within a specified radius are grouped into a cluster, with its X and Z positions corresponding to the median of the sources; clusters with fewer solutions than specified by the user are rejected. After some trials, a minimum of 30 solutions within a radius of 1000 m were retained for clustering.

In Fig. 3(b), the thin-sheet clusters are clearly deeper than the contact-type ones; this is in accordance with what was first experienced on synthetic models by Hartman *et al.* (1971). Also, the thin-sheet solutions clearly fit better with what was previously known of the basement geometry, derived from

boreholes (Fig. 3b). This can also be explained by synthetic results from Hartman *et al*. (1971): the contact-type sources provide more accurate depth estimates for shallow sources (when the vertical extent of the source cannot be neglected in comparison to its depth), whereas the thin-sheet model provides better estimations for deeper sources. As a consequence, the true depth of the magnetic source is generally between the depths computed using the two models. A review of the computed Werner clusters along the profiles of Région Centre shows that thin-sheet Werner solutions are almost always below or close to the borehole basement surface, whereas contact-type sources very often fall within the basin; this is illustrated on a specific profile in Fig. 3(b).

Based on this observation and with the objective of picking the top of the basement in Werner clusters, a selection of the uppermost Werner thin-sheet solutions was performed. This was achieved using a moving window algorithm (on the whole map – not along the flight lines): the shallowest Werner clusters found in a 1500 m square window moving every 500 m were retained. The initial number of thin-sheet clusters obtained in the area of study is 12 667, out of which 967 uppermost clusters were extracted. Among the superficial clusters, only 9 are clearly located within the basin, well above the borehole basement surface and were therefore rejected. An example of the extracted uppermost Werner clusters is shown in Fig. 3(c); in this figure, some sources look close to the basement surface but are not selected: this is because shallower sources should exist in adjacent profiles (within the 1500 m square window). On the contrary, due to the automatic picking of shallow sources, some isolated sources within the basement could probably be erroneously picked, thus introducing some apparent local deepening of the basement top. However, this effect is not obvious in the basement map (Fig. 4).

Interpolation of Werner magnetic sources

Because only the shallowest magnetic sources were sampled all over the study area, it is straightforward to derive a map of the magnetic basement top by interpolation of source depths. In order to derive a magnetic basement surface coherent with both Werner sources and the magnetic structural sketch map, the magnetic discontinuities (Fig. 1) were taken into account during the interpolation. Indeed, magnetic discontinuities (not magnetic structures) reveal ruptures in magnetic anomalies that are basically interpreted as faults. As such, if Werner sources on both sides of a discontinuity are at different depths, the discontinuity-driven interpolation produces a rupture in the magnetic basement surface. Interpolation was performed by kriging with a linear variogram and zero drift; it properly takes into account discontinuities, while data are respected. The interpolated magnetic basement surface is shown in Fig. 4; it also takes into account the depth of the basement documented in the 41 boreholes scattered throughout the study area (see their location in Fig. 4), as well as the outcropping limits of the basement.

The obtained magnetic basement map is consistent with the overall geometry of the Paris Basin, which is developed along the Armorican massif and the Massif Central basement to the west and south respectively and deepens towards the northeast. Altogether, deepening of the basin occurs along the three previously mentioned N150E discontinuities, which seem to accommodate the opening of the south-western part of the Paris Basin in a series of steps along which dextral slip is also visible on the magnetic map.

At the regional scale, the Werner magnetic basement compares well to the basement surface previously interpolated using the deep boreholes only (contours in Fig. 4; Chantraine *et al*. 1996). The main differences occur in the south and south-eastern part of the map, where the magnetic basement displays more variations and structures than had previously been recognized. It must be recalled that this map of the magnetic basement is not intended to represent a detailed geometry of the geological basement since Werner magnetic sources are theoretically within the basement (even if close to its surface) because they derive from geological variations that occur within the basement (reaching its surface sometimes). The downward spreading of Werner sources (inherent to the method) also tends, while clustering, to slightly overestimate the depth of clusters. However, the relative variations of depth of the magnetic sources, at the scale of the map, should provide a good indication of the topography of the basement. Nonetheless, in the southern part of the map where the basement is shallower, using the thin-sheet source model, the depth of the magnetic basement is probably somewhat overestimated. Also, in the south-western part of the map, where more Werner sources are grouped, some local depth variations occur. Detailed line-to-line analysis of these slight depth variations shows that their amplitude is of the order of 100 m to a maximum of 200 m; this reveals the limit of accuracy of the method. The various causes for this include: 1) Werner deconvolution assumes 2D structures perpendicular to the profiles (which is not truly the case), 2) for shallow depths, the thin-sheet model may not be optimal and 3) in areas where Werner sources are numerous, the algorithm of extraction of the shallowest Werner sources can sometimes not be sophisticated enough, accepting some slightly deeper sources together with the shallowest ones.

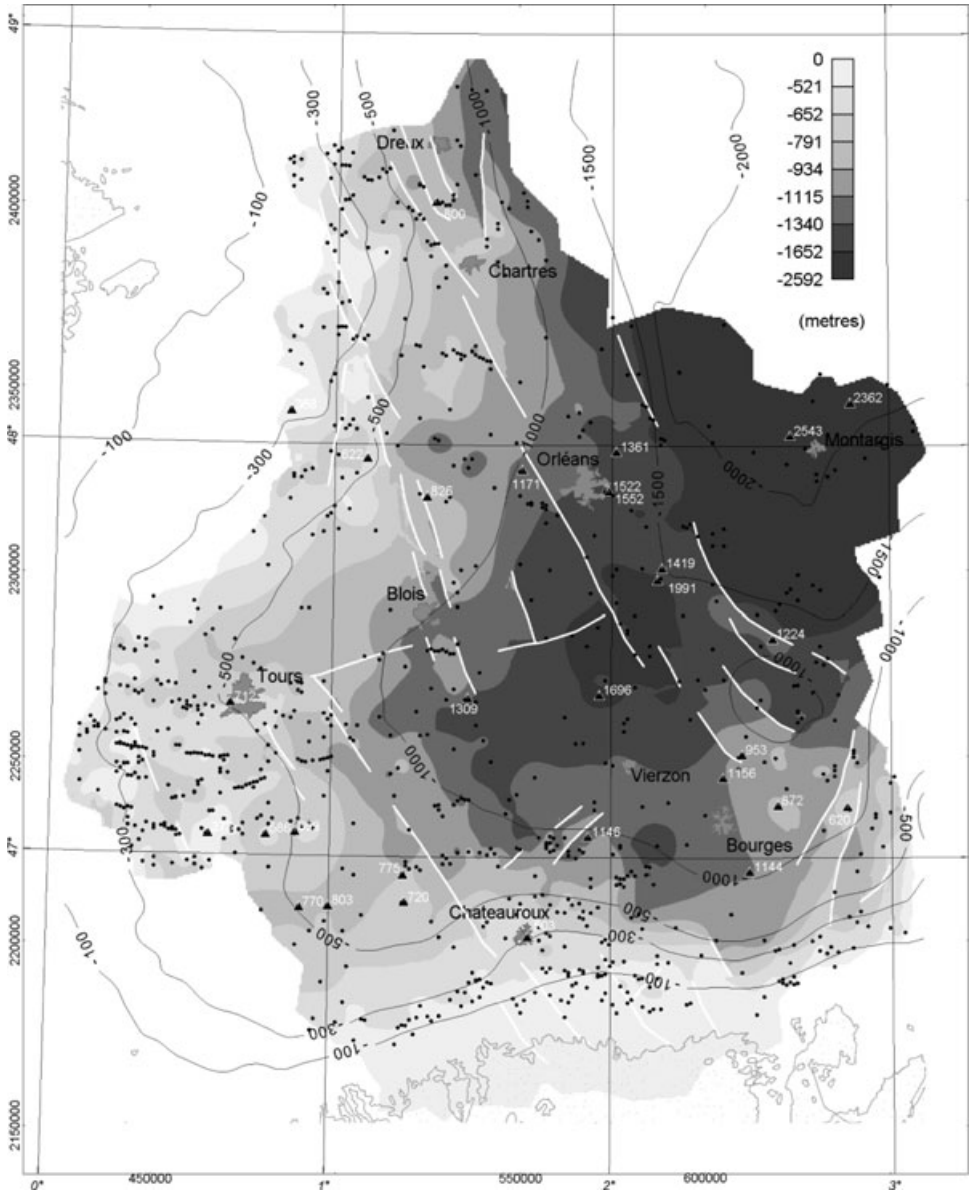

Figure 4 Map of the interpolated Werner magnetic basement (grey tones) obtained by interpolation of Werner sources (black dots) together with deep boreholes (triangles) and taking into account the magnetic structures interpreted in Fig. 1 (white lines). For comparison: previously existing basement interpolated from drill holes only (black contours) (Chantraine *et al*. 1996).

GEOPHYSICAL SIGNATURES OF THE BASEMENT

Several previous studies have investigated the nature of the basement of the Paris Basin using gravity and magnetic data. They all shared the basic idea that the gravity and magnetic effects of basement rocks should be 1) recorded in the surface measurements, 2) combined in order to retrieve characteristic geophysical signatures and 3) manually interpreted in terms of probable lithology with regard to rock petrophysical characteristics and basement nature documented in boreholes.

In the following paragraphs we review these assumptions and develop the approach we chose in order to map the geophysical signatures of the basement: in particular, we adopt a noticeably different approach in order to interpret the data, based on a numerical classification of the gravity and magnetic maps, instead of manual interpretation. On the other hand, our interpretation is not lithological but petrophysical

instead; that is to say, at this stage we use the borehole information for discussion only. The purpose of the present work is to show what can be achieved using potential fields; the final work of the integration of our results together with borehole information and detailed seismic interpretation is beyond the scope of this paper and shall be addressed in a distinct more interpretative publication.

Concerning the first assumption, previous publications have very clearly shown that the petrophysical characteristics (i.e., density and magnetic susceptibility) of the basement rocks surrounding the basin or measured on drill-hole samples vary significantly (e.g., Weber 1968; Corpel and Debeglia 1988) and can be traced out beneath the sedimentary cover (e.g., Weber 1973).

Concerning the second assumption, all previous studies have recognized the fact that the sedimentary infilling is almost 'transparent' for the magnetic field (i.e., almost all the magnetic signal recorded at the surface derives from the basement, Weber 1973), whereas the gravity field contains both the effect of the basement and of the basin. The 'perturbing' gravity effect of the sediments has then to be removed in order to address density variations in the basement. When the geometry and density variations within the sedimentary pile are sufficiently well-known (from seismic data and borehole diagraphies – Heritier and Villemin 1971; Guillocheau *et al*. 2000), the gravity effect of the basin can be subtracted (i.e., stripped) from the Bouguer anomaly (Corpel and Debeglia 1988; Guillocheau *et al*. 2000). In the Paris Basin, as shown in Fig. 2, the gravity effect of the sedimentary infilling (after Corpel and Debeglia 1988) is relatively smooth and thus, some older publications simply neglected the gravity effect of the sediments (e.g., Weber and Lorne 1966; Weber 1971). An alternative is to consider that the vertical gradient of the Bouguer anomaly can properly attenuate the smooth effect of the sedimentary pile (Debeglia and Weber 1985). We chose this solution: indeed, the vertical gradient operator enhances local anomalies, while removing the regional wavelengths of the field. And actually, the vertical gradient gravity map compares very well to the stripped anomaly (from Corpel and Debeglia 1988) (respectively grey-shades compared to contours in Fig. 2). The vertical gradient has the advantage of being straightforward to obtain and also to provide a more detailed outline of the density contrasts.

The magnetic map we used for classification was chosen following two considerations: 1) it had to render as detailed information of the structure and magnetization of the basement as possible, 2) it had to be physically as homogeneous as possible with the gravity first vertical derivative. The magnetic map reduced to the pole fulfils the second condition but not the first one: the preeminent effect of the PBMA (trending N-S, along the eastern border of the map) largely interferes and masks surrounding magnetic contrasts (as pointed out by Weber 1971). The vertical derivative of the magnetic map fulfils the first condition but not the second. The alternative we chose was to filter the magnetic anomaly reduced to the pole with a 15 km high-pass Butterworth filter. While keeping the properties of the reduction to the pole, this effectively removed long wavelength undesired effects. We recall that this was suitable to highlight magnetic properties of the basement since it was previously recognized that the sedimentary cover is mostly non-magnetic (Weber 1973). Conversely, several bimodal anomalies related to remnantly magnetized geological bodies remain and obscure the interpretation: the analytical signal could have been used instead, simplifying the reading of the magnetizations but this map was not homogeneous with the first vertical derivative of the gravity and also did not provide good structural detail.

In order to obtain a joint pseudo-lithological interpretation of the gravity and magnetic data, we combine the gravity vertical gradient and the filtered magnetic anomaly reduced to the pole into a numerical classification, instead of manual interpretation. This is achieved using standard unsupervised isodata clustering (e.g., Venkateswarlu and Raju 1992): based on their magnetic and gravity signatures, all the pixels of the map are statistically distributed among a user-defined number of clusters. Nine classes were finally retained, corresponding to a categorization of the clusters with respect to 3×3 levels of density and magnetization (Fig. 5). Visually, these clusters define three main ensembles distinguished by their gravity signature and outlined by their magnetic property. The map of Fig. 5 exhibits very coherent spatial distributions of the petrophysical properties, which look even more coherent in light of the magnetic structures interpreted in Fig. 1. It is noticeable that some structures that had not been traced out in the magnetic map are revealed by the association with gravity data; for instance, the Sennely fault that was not visible in the magnetic map is now clearly evidenced (drawn in Fig. 5, along a N-S direction east of Orléans). It is in good correspondence with its position confirmed by seismic data.

In Fig. 5, in the western part of the map, well-defined N120E structured trends are evidenced, which we interpret as the extension of trends of the basement outcropping further to the west in the Armorican massif. Where they outcrop, these alternations are composed mostly of (i) low-density/low-magnetization Neoproterozoic to Paleozoic metasediments and acid plutonic rocks, (these correspond to the pink tones in

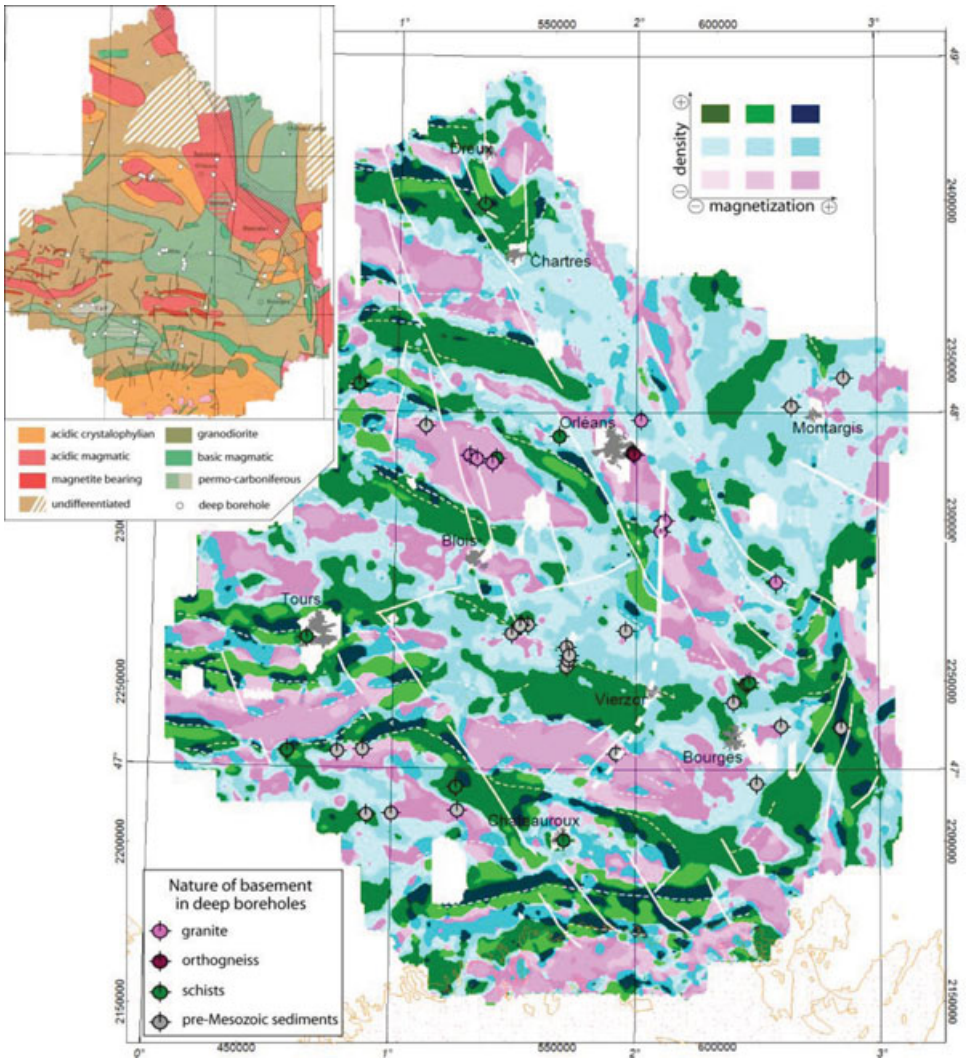

Figure 5 Map of the petrophysical signatures within the basement resulting from the classification of magnetic (magnetic anomaly reduced to the pole and 15 km high-pass filtered) and gravity signatures (vertical gradient of the Bouguer anomaly), together with the nature of the basement in deep boreholes. Magnetic trends and discontinuities are superimposed (respectively white dashed and plain lines). It is noticeable that the Sennely fault (white bold plain line trending N-S, east of Orléans) can be traced out (contrary to Fig. 1, with magnetism only), in accordance with its existence attested by seismic data. In the insert an existing predictive basement map (after Mégnien 1980) is provided for comparison (see text for comments).

Fig. 5) and (ii) higher density/magnetization crystallophylian, basic plutonic or volcanogenic rocks (these correspond to the green tones in Fig. 5). This part of the map is well correlated with borehole information. To the east, these alternations are sharply interrupted along two well-expressed N150E to N170E structural discontinuities. The northern discontinuity runs from Chartres to the south of Orléans; it is apparently 'connected' to the southern discontinuity by a conjugate N75 discontinuity towards Tours. The southern discontinuity passes nearby Chateauroux and seems to be interrupted at its southern end along a dense and magnetic E-W elongated body, previously interpreted as granodioritic (e.g., Weber 1973). Displacement along the two N150E to N170E discontinuities can be visually identified (Figs 1 and 5): the dextral slip is particularly well expressed by the displacement of about 40 km of several magnetic markers along the southern discontinuity. Along the northern discontinuity, a dextral slip also occurs, apparently with a higher displacement (around 60 km) and the magnetic markers displaced towards the south-east are apparently also folded against what was previously recognized as a major basement domain boundary (e.g., Autran *et al.* 1994), along the 'faille de la Loire' that lines the east

of PBMA. This eastern part of the map is well structured but except for the PBMA itself, patterns of petrophysical contrasts are not displayed as clearly as in the west. In particular, east of the PBMA, low-magnetic and gravity contrasts might suggest a somehow different nature of the basement than west of the PBMA, supporting the idea that the PBMA might mark a limit in the basement nature (e.g., Weber 1971; Autran *et al*. 1994). This will have to be confirmed if new high-resolution aeromagnetic data become available east of Région Centre.

DISCUSSION

Among the information that potential field data can provide, the most notable result in this study is the regional structural sketch. As already evidenced, the sediments that constitute the Paleozoic to Cenozoic infilling of the Paris Basin can, to the first order, be considered as magnetically transparent (e.g., Autran *et al*. 1994) and thus most of the magnetic signal originates from the crystalline basement underneath. However, it must also be noted that most of the structures that affect the sedimentary cover are reactivated from ancient basement structures (e.g., Autran *et al*. 1994). With this in mind, the magnetic vertical gradient map (Fig. 1) brings invaluable new information on basement structures (structural trends displayed as white lines in Fig. 1). The main trends in the new magnetic map are: 1) a detailed outline of the well-known 'Paris Basin Magnetic Anomaly' (PBMA), elongated N-S to N150E along the east of the map, 2) E-W to WNW trends on the western part of the map, which are the extension of Armorican trends outcropping further to the west and 3) cross-cutting previous trends, several great magnetic discontinuities oriented N140E to N150E.

The N150E structural direction is known throughout the Armorican massif, expressed in the topography by alignments of small tertiary basins that were developed reactivating Permo-Triassic fracture zones related to the opening of the northern Atlantic Ocean (Vigneresse 1988). In the magnetic map of Région Centre, the basement is split into four main compartments along these structures. The N150E discontinuities have two visible effects highlighted by our processing: either dextral shear or vertical movement. Dextral shear is visible for instance south of Tours (as evidenced in Figs 1 and 5), where three E-W magnetic trends are cross-cut by a N150E discontinuity and can be traced out about 40 km further to the south-east. Vertical movement is revealed by the attenuation and spreading of the magnetic anomalies from west to east (Fig. 1), which attests for the deepening of the magnetic basement (Fig. 4). This combined dextral and normal kinematics is strikingly consistent with what was described by Vigneresse (1988), primarily in Brittany and extended in England and Ireland. It was interpreted as a Permian to Aptian fault system, that was 700 km wide and striking N130E to N150E, which was related to the opening of the North Atlantic Ocean, with some evidence that it probably reactivated older structures.

However, the structural information highlighted by magnetic data is of course not exhaustive. For instance, the Sennely fault, trending N-S, east of Orléans (see location in Fig. 5) has a known 500 m vertical offset at the basement level, documented by seismic data as well as by two closely spaced boreholes. This fault has no apparent magnetic expression (Fig. 1); Werner magnetic clusters, however (Fig. 4), suggest a geometry of the basement compatible with this offset (see SE of Orléans around drill holes at 1419 and 1991 m). Conversely, some of the magnetic gradients might not be associated with vertical displacements of the basement top and their use during interpolation of Werner sources is therefore not optimal. Meanwhile, the interpretation of magnetic trends, textures and discontinuities, provides an original overview of regional magnetic structures, some of which were previously unknown. As pointed out in Fig. 5, the combination of magnetism with gravity further enhances the interpretation, as is shown, for instance, with the Sennely fault, which is clearly outlined in Fig. 5. Following the same idea, it is clear that a future detailed integration of potential fields together with seismic data and a detailed analysis of borehole data can provide an optimal description of deep basement/basin relations.

In the present paper nothing has been said about the Permo-Carboniferous basins that are considered as part of the Pre-Mesozoic basement. The presence of such basins is confirmed in several drill holes, mostly in the southern half of the region (Fig. 5) and has tentatively been interpreted in some seismic lines that suggest that their thickness reaches in some places several kilometres but their extension is still largely under debate. Correlation of these Permo-Carboniferous basins (insert, Fig. 5) with the gravity/magnetic signatures of the basement in Fig. 5 is not straightforward and at this stage it would be too hypothetical to interpret the magnetic /gravity data alone, in terms of buried Paleozoic basins. What can however be noted from our Werner sources is that in areas where Paleozoic basins are probable (Fig. 5), the depth of the magnetic sources does not significantly increase; this suggests that the Paleozoic basins may contain magnetic material. This is in accordance with the volcanic nature of Permo-Carboniferous deposits recognized both in drill holes and in Paleozoic basins outcropping around the Paris Basin (e.g., Chateauneuf and Farjanel 1989). A detailed modelling of the gravity and

magnetic data with petrophysical and seismic constraints should significantly improve the knowledge of the geometry and nature of the Pre-Mesozoic basement. In our opinion, opening of these basins will prove to be controlled along some of the major magnetic discontinuities revealed by our study.

Concerning the magnetic basement-depth map derived here, some comments need to be formulated on the choice and limits of the method used. Indeed, Werner deconvolution has long been used to characterize the magnetic basement (see elements of review in Nabighian *et al*. 2005). However, the method has been used in several significantly different ways: originally, Hartman *et al*. (1971) derived a few solutions, each solution being associated to a single anomaly; interpretation in terms of basement depth was straightforward. Then with multiple-source Werner deconvolution (Hansen and Simmons 1993), a much larger number of sources were derived and several strategies were developed in order to interpret them. Some authors simply delineated the basement interface by visual identification of clustered sources (e.g., Davy and Wood 1994). Several publications have proposed advanced numerical clustering of solutions applicable for Euler and Werner deconvolutions, using for instance kernel density algorithms (Ugalde and Morris 2010), artificial intelligence (Mikhailov *et al*. 2003) or Marquardt's modelling (Ku and Sharp 1983). But most authors (e.g., Balia *et al*. 1991; Bell *et al*. 2006), in the same way as we did, have been using simple clustering with the aim of grouping significant clusters of solutions and rejecting disseminated ones (considered as less reliable). Some authors have also clustered Werner solutions and then visually identified the characteristic patterns of solutions to delineate the basement (Goussev and Peirce 2010). The method adopted here, although not extremely sophisticated, has proven to bring reliable results in cases where independent control data were available (e.g., Davy and Wood 1994; Studinger *et al*. 2003). But, as noticed by several authors, this is true as long as the data are correctly prepared (high-frequency noise should be avoided) and with some experience and trial and error, to achieve a proper tuning of the deconvolution and subsequent clustering. In Région Centre, proper tuning of Werner deconvolution was attested by the good correspondence of Werner clusters with the depth of basement recorded in deep petroleum boreholes (Fig. 3). Accordingly, interpolation of the top Werner clusters together with borehole basement depths resulted in a map of the basement, with no clear evidence of inconsistency between the boreholes and Werner sources (i.e., no interpolation 'bubbles' around the boreholes in Fig. 4). We also present along two cross-sections going through several boreholes (Fig. 6), the projection of Werner clusters (located within 1 km of the profiles) and the interpolated magnetic basement surface – we recall that the interpolation takes into account the boreholes and Werner clusters. Again, Werner sources and borehole data have an overall good consistency and the geometry of the interpolated surface looks realistic. This result certainly does not prove that the derived basement surface is exact but at least it is coherent with available boreholes and provides us with a map displaying realistic patterns. In order to evaluate the feasibility of a future integration of Werner sources with available seismic data, a test of the coherence between both data sets was attempted along an E-W profile cross-cutting the bulge of the basement previously pointed out by Euler sources, south of the area of study (see location of the profile in Fig. 1). In Fig. 7, interpretation of the seismic data as well as the depth-velocity conversion are preliminary, based on two boreholes: the basement / Mesozoic sediment interface was interpreted together with the presence of a Pre-Mesozoic sedimentary basin confirmed in an Arpheuilles borehole. Werner clusters within 1 km of the section were projected onto the profile. The basement bulge is well expressed both in the seismic data and in Werner clusters. Their depth and geometry are, at the first order, in fairly good correspondence. It is also noticeable that in the Pre-Mesozoic part of the basement Werner clusters are less numerous and their depth is also more difficult to interpret: neither at the top nor at the bottom of the basin. This is probably related to the overall low magnetism of these terranes, with possibly some intercalated magnetic layers of volcanic deposits. Altogether, this preliminary cross-visualization of magnetic and seismic information at the basement level supports the use of joint interpretation in order to attempt mapping of the basement of such basins.

The last step of processing proposed in this paper in order to achieve a fast preliminary mapping of petrophysical gravity/magnetic characteristics of the basement, was achieved through a very straightforward unsupervised classification. This approach was proposed as a way to quickly combine gravity and magnetic information and to simply visualize first-order petrophysical patterns of the basement, below the basin. The adopted procedure is definitely not intended to provide a detailed mapping of the actual density/magnetic contrasts of the basement; this would require much more sophisticated processing, including detailed evaluation/filtering of the magnetic contribution of the basin, stripping of the gravity effect of the sediments and conversion of gravity/magnetic residual signatures in pseudo density/magnetization. This was already attempted in the Paris Basin using older gravity/magnetic data and taking into account regional seismic models of the

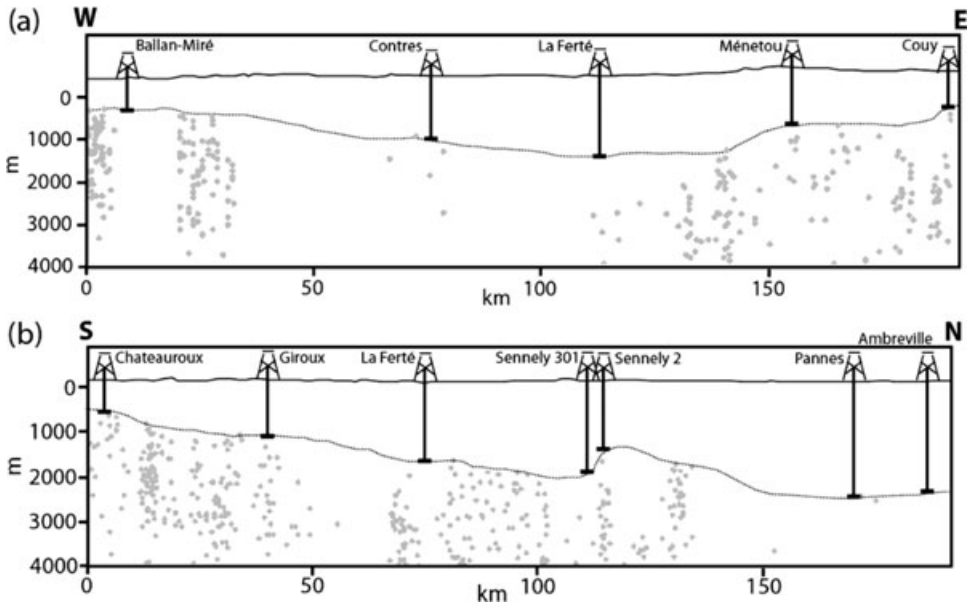

Figure 6 Two cross-sections displaying the basement top as documented in boreholes (dash at the base of the boreholes) together with Werner clusters (grey dots) and our interpolated magnetic basement top. Location of the profiles is displayed as thick black lines in Fig. 1: (a) the W-E profile cross-cutting the centre of the map; (b) the S-N profile located along the western border of the map. Werner clusters located within 1 km of the section were projected onto the profile.

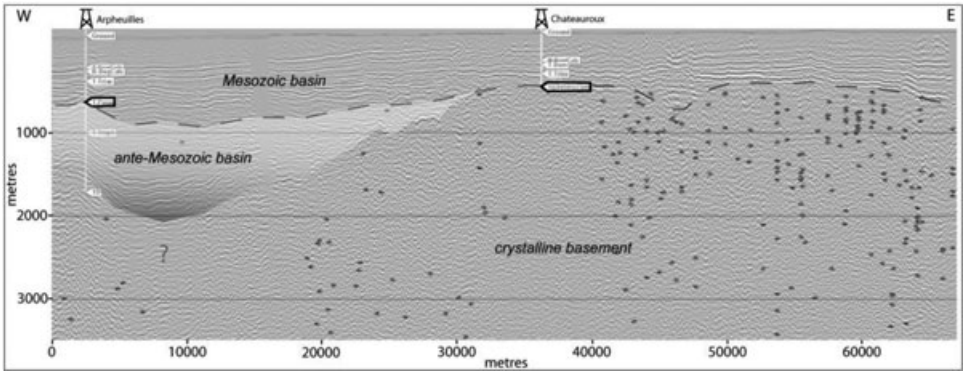

Figure 7 W-E oriented seismic section cross-cutting the 'magnetic bulge' located south of the study area (see the location of the section in Fig. 1). Werner magnetic sources (grey dots) located within 1 km of the section were projected onto the profile. Black arrows on two deep boreholes locate the top of the Pre-Mesozoic basement. This basement can be crystalline (right part of the figure) or can be sedimentary such as in the Arpheuilles basin (grey shade, left of the figure). See text for further comments.

sedimentary pile (Corpel and Debeglia 1988; Guillocheau *et al*. 2000). As an alternative, combining suitable gravity and magnetic maps, proved to provide a classification result in very good agreement with previous studies. In some places, the classification map revealed new information compared to existing predictive basement maps (Mégnien 1980; Debeglia and Weber 1985), due to the use of more accurate data and also because appropriate processing was used to focus the anomalies, while removing the regional wavelengths of the field. In order to produce a new detailed basement map, Fig. 5 would further need to be carefully interpreted together with the information reported in deep boreholes and, where available, integrating seismic information of buried Pre-Mesozoic basins to be tested in forward 2.5D modelling of the gravity/ magnetic data.

CONCLUSIONS

The purpose of this paper was to show how much can be extracted from a fast analysis of potential field data

(aeromagnetic and gravity data) in terms of structure, geometry and nature of the basement underneath sedimentary basins. In the basin environment, since the sedimentary pile is often almost non-magnetic, the magnetic structural sketch map provides a unique insight into the tectonics of the buried basement and consequently in the regional geodynamics. Through a case study in the SW Paris Basin, the paper also discusses the limits of this exercise and re-assesses the necessity of a follow-up study involving independent data such as seismic, boreholes, etc. to strengthen the use of such data for a detailed assessment of a buried basement underneath large basins.

First, the structure and geometry of the basement were addressed. Processing was divided into three stages in order to derive a realistic geometry of the magnetic basement: 1) the main structures of the magnetic basement were highlighted using Euler deconvolution and interpreted in a structural sketch map, 2) Werner deconvolution and ad hoc post-processing allowed the extraction of a set of magnetic sources at (or close to) the magnetic basement and 3) these sources, together with the available depth of basement in the boreholes were interpolated taking into account the structures, in order to provide a 3D surface of the magnetic basement.

In Région Centre, within the Paris Basin, the new high-resolution aeromagnetic map actually offers a continuous view of regional basement structures and reveals still poorly known and complex deformations at the junction between major domains of the Variscan collision belt. Specifically, a series of three previously unknown great magnetic discontinuities oriented N140E to N150E outstandingly structure the basement. The geometry of the Werner magnetic basement interpolated together with the magnetic structural sketch provides a map displaying realistic patterns, coherent with basement depths available in deep petroleum boreholes.

In addition, a fast mapping of the petrophysical characteristics of the basement was achieved by unsupervised classification of suitably selected gravity and magnetic maps. This procedure provides an integrated overview of magnetic/gravity-induced patterns of the basement. Deriving a predictive lithological map of the basement was beyond the scope of this article but this would require a minimal effort, interpreting the petrophysical map derived here, together with basement lithology reported in deep boreholes and, if available, integrating deep seismic information concerning possible buried Pre-Mesozoic basins. With some additional petrophysical information derived from drill cores, a most detailed analysis of the basin/basement attainable by indirect methods would be achieved by forward 2D and/or 3D modelling of the gravity/magnetic data.

ACKNOWLEDGEMENTS

We thank Alan Reid, John Peirce and Giovanni Florio for their questions and comments that undoubtedly contributed to improve the manuscript. Agnès Martelet is kindly thanked for her help in editing the manuscript. The airborne geophysical data used in the study were co-financed by Région Centre, BRGM and FEDER European funds. Figures of the article were produced with Geosoft© software.

REFERENCES

Autran A., Lefort J.P., Debeglia N., Edel J.B. and Vigneresse J.L. 1994. Gravity and magnetic expression of terranes in France and their correlation beneath overstep sequences. In: *Pre-Mesozoïc geology in France and related areas*, (ed. J.D. Keppie), Springer-Verlag, Berlin Heidelberg.

Balia R., Fais S., Klingele E., Marson I. and Porcu A. 1991. Aeromagnetic constraints on the geostructural interpretation of the southern part of the Sardinian Rift, Italy. *Tectonophysics, The European Geotraverse Part 7* **195**, 347–358.

Barbosa V.C.F., Silva J.B.C. and Medeiros W.E. 1999. Stability analysis and improvement of structural index estimation in Euler deconvolution. *Geophysics* **64**, 48–60.

Bayer R., Guillen A. and Rousset D. 1988. Réactualisation de l'interprétation de l'AMBP sur la région de Couy-Sancerre. In: *Forage scientifique de Sancerre-Couy (Cher), données géophysiques préliminaires*, (ed. C. Weber) pp. 167–178. Documents BRGM 138, Orléans, France.

Bell R., Studinger M., Karner G.D., Finn C. and Blankenship D. 2006. Identifying major sedimentary basins beneath the West Antarctic Ice Sheet from aeromagnetic data analysis. In: *Antarctica: Contributions to Global Earth Sciences*, (eds D.K. Fütterer *et al.*), pp. 117–121. Springer, Berlin.

Bosch M., Guillen A. and Ledru P. 2001. Lithologic tomography: An application to geophysical data from the Cadomian belt of Northern Brittany, France. *Tectonophysics* **331**, 197–228.

Chantraine J., Autran A., Cavelier C., Alabouvette B., Barféty J.-C. and Cecca F. 1996. *Carte Géologique de la France à L'échelle du Millionième*. BRGM (6ème édition), Orléans, France.

Chateauneuf J.J. and Farjanel G. 1989. In: *Synthèse géologique des bassins permiens français*, (ed. Mémoire du BRGM 128) p. 28. Orléans, France.

Corpel J. and Debeglia N. 1988. Étude bassin de Paris-Centre: Réinterprétation des données gravimétriques et magnétiques. Rapport BRGM 88 DT 021 GPH.

Davy B. and Wood R. 1994. Gravity and magnetic modelling of the Hikurangi Plateau. *Marine Geology* **118**, 139–151.

Debeglia N. and Corpel C. 1997. Automatic 3-D interpretation of potential field data using analytic signal derivatives. *Geophysics* **62**, 87–96.

Debeglia N. and Weber C. 1985. Geologic mapping of the basement of the Paris basin (France) by gravity and magnetic data interpretation. In: *The Utility of regional gravity and magnetic anomaly maps*, (ed. W.J. Hinze). SEG.

Galdeano A. and Guillon J.C. 1988. Interprétation des données magnétiques et gravimétriques. In: *Etude de la croûte terrestre par sismique profonde – Profil Nord de la France, structure hercynienne*, (eds M. Cazes and G. Toreilles). Technip.

Gérard A. 1971. Apports de la gravimétrie à la connaissance de la tectonique profonde du bassin de Paris. *Bulletin du BRGM*, 2e série, **2**.

de Gery Chastenet T. and Naudy H. 1957. Sur l'interprétation des anomalies gravimétriques et magnétiques. *Geophysical Prospecting* **5**, 421–448.

Goussev S.A. and Peirce J.W. 2010. Magnetic basement: Gravity-guided magnetic source depth analysis and interpretation. *Geophysical Prospecting* **58**, 321–334.

Guillen A., Bayer R., Million R. and Rousset D. 1990. Évolution des hypothèses et modélisations pour l'interprétation de l'anomalie magnétique du bassin de Paris (région de Sancerre). *Bulletin de la Societe Géologique de France*, **VI**(5), 739–748.

Guillen A., Calcagno P., Courrioux G., Joly A. and Ledru P. 2008. Geological modelling from field data and geological knowledge, Part II. Modelling validation using gravity and magnetic data inversion. *Physics of the Earth and Planetary Interiors* **171**, 158–169.

Guillen A. and Menichetti V. 1984. Gravity and magnetic inversion with minimization of a specific functional. *Geophysics* **49**, 1354–1360.

Guillocheau F., Robin C., Allemand P., Bourquin S., Brault N., Dromart G. *et al*. 2000. Meso-Cenozoic geodynamic evolution of the Paris Basin: 3D stratigraphic constraints. *Geodinamica Acta* **13**(4), 189–245.

Gunn P.J. 1997. Quantitative methods for interpreting aeromagnetic data: A subjective review. *AGSO Journal of Australian Geology and Geophysics* **17**, 105–113.

Hansen R.O. 2005. 3D multiple-source Werner deconvolution for magnetic data. *Geophysics* **70**, 45–51.

Hansen R.O. and Simmonds M. 1993. Multiple-source Werner deconvolution. *Geophysics* **58**, 1792–1800.

Hartman R.R., Teskey D.J. and Friedberg J.L. 1971. A system for rapid digital aeromagnetic interpretation. *Geophysics* **36**, 891–918.

Hassan H.H., Peirce J.W., Pearson W.C. and Pearson M.J. 1998. Cultural editing of HRAM data, comparison of techniques. *Canadian Journal of Exploration Geophysics*, n° 1 and 2, **34**, 16–22.

Héritier F. and Villemin J. 1971. Mise en évidence de la tectonique profonde du Bassin de Paris. *Bulletin de la Societe Géologique de France* **2**, 11–30.

Hsu S.-K., Coppens D. and Shyu C.T. 1998. Depth to magnetic source using the generalized analytic signal. *Geophysics* **63**, 1947–1957.

Huang D. 1996. *Enhancement of automatic interpretation techniques for recognising potential field sources*. PhD thesis, University of Leeds, UK.

Joly A., Martelet G., Chen Y. and Faure M. 2008. A multidisciplinary study of a syntectonic pluton close to a major lithospheric-scale fault: Relationships between the Montmarault granitic massif and the Sillon Houiller Fault in the Variscan French Massif Central. Part II: Gravity, aeromagnetic investigations and 3D geologic modelling. *Journal of Geophysical Research* **113**, B01404.

Keating P.B. 1998. Weighted Euler deconvolution of gravity data. *Geophysics* **63**, 1595–1603.

Ku C.C. and Sharp J.A. 1983. Werner deconvolution for automated magnetic interpretation and its refinement using Marquardt's inverse modelling. *Geophysics* **48**, 754–774.

Le Borgne E. and Le Mouel J.L. 1966. La nouvelle carte magnétique de la France. Note IPG n° 15.

Li X. 2003. On the use of different methods for estimating magnetic depth. *The Leading Edge* **22**, 1090–1099.

Lorenz C., Mégnien C., Weber C., Bergerat F., Boulègue J., Burg J.P. *et al*. 1987. Premiers résultats du sondage implanté sur l'anomalie magnétique du bassin de Paris, au sud de Sancerre (Cher), Programme géologie profonde de la France. *Comptes Rendus de L' Académie des Sciences, Paris, série II* **305**, 1099–1104.

Marello L., Ebbing J. and Gernigon L. 2010. Magnetic basement study in the Barents Sea from inversion and forward modelling. *Tectonophysics* **493**, 153–171.

Marson I. and Klingele E.E. 1993. Advantages of using the vertical gradient of gravity for 3-D interpretation. *Geophysics* **58**, 1588–1595.

Martelet G., Calcagno P., Gumiaux C., Truffert C., Bitri A., Gapais D. and Brun J.P. 2004. Integrated 3D geophysical modelling of the Hercynian Suture Zone in the Champtoceaux area (south Brittany, France). *Tectonophysics* **382**, 117–128.

Martelet G., Debeglia N. and Truffert C. 2002. Updating and validating the French gravity terrain corrections out to a distance of 167 km. *Comptes Rendus Geoscience* **334**, 449–454.

Martelet G., Pajot G. and Debeglia N. 2009. Nouvelle carte gravimétrique de la France; RCGF09 – Réseau et Carte Gravimétrique de la France, 2009. Rapport BRGM/RP-57908-FR, 77 pp.

Martelet G., Sailhac P., Moreau F. and Diament M. 2001. Characterization of geological boundaries using 1-D wavelet transform on gravity data; Theory and application to the Himalayas. *Geophysics* **66**, 1116–1129.

Mégnien C. 1980. Synthèse géologique du Bassin de Paris. *Mémoire du BRGM*, 102.

Mikhailov V., Galdeano A., Diament M., Gvishiani A., Agayan S., Bogoutdinov S. *et al*. 2003. Application of artificial intelligence for Euler solutions clustering. *Geophysics* **68**, 168–180.

Moreau F., Gibert D., Holshcneider M. and Saracco G. 1997. Wavelet analysis of potential fields. *Inverse Problems* **23**, 165–178.

Mushayandebvu M.F., van Driel P., Reid A.B. and Fairhead J.D. 1999. Magnetic imaging using extended Euler deconvolution. 69th Annual International Meeting, Society of Exploration Geophysicists.

Nabighian M.N. 1972. The analytic signal of two-dimensional magnetic bodies with polygonal cross-section. *Geophysics* **37**, 507–517.

Nabighian M.N., Grauch V.J.S., Hansen R.O., LaFehr T.R., Li Y., Peirce J.W. *et al*. 2005. The historical development of the magnetic method in exploration. *Geophysics* **70**, 33ND.

Nabighian M.N. and Hansen R.O. 2001. Unification of Euler and Werner deconvolution in three dimensions via the generalised Hilbert transform. *Geophysics* **66**, 1805–1810.

Oldenburg D.W. 1974. The inversion and interpretation of gravity anomalies. *Geophysics* **39**, 526–536.

Perrin J., Martelet G., Truffert C. and Deparis J. 2009. Acquisition géophysique aéroportée de la région Centre, Phase 1 – Magnétisme et radiométrie spectrale. Rapport BRGM RP-57442-FR.

Peters L.J. 1949. The direct approach to magnetic interpretation and its practical application. *Geophysics* **14**, 290–320.

Phillips J.D. 1997. Potential-Field Geophysical Software for the PC, version 2.2. USGS open-file report, pp. 97–725.

Reid A.B., Allsop J.M., Granser H., Millett A.J. and Somerton I.W. 1990. Magnetic interpretation in three dimensions using Euler deconvolution. *Geophysics* **55**, 80–91.

Roest W.R., Verhoef J. and Pilkington M. 1992. Magnetic interpretation using the 3-D analytic signal. *Geophysics* **57**, 116–125.

Sailhac P., Galdanéo A., Gibert D., Moreau F. and Delor C. 2000. Identification of sources of potential fields with the continuous wavelet transform: Complex wavelets and application to aeromagnetic profiles in French Guiana. *Journal of Geophysical Research* **105**, 19455–19475.

Stavrev P.Y. 1997. Euler deconvolution using differential similarity transformations of gravity or magnetic anomalies. *Geophysical Prospecting* **45**, 207–246.

Studinger M., Bell R.E., Karner G.D., Tikku A.A., Holt J.W., Morse D.L. *et al*. 2003. Ice cover, landscape setting, and geological framework of Lake Vostok, East Antarctica. *Earth and Planetary Science Letters* **205**, 195–210.

Talbot J.Y., Martelet G., Courrioux G., Chen Y. and Faure M. 2004. Emplacement in an extensional setting of the Mont Lozère–Borne granitic complex (SE France) inferred from comprehensive AMS, structural and gravity studies. *Journal of Structural Geology* **26**, 11–28.

Thompson D.T. 1982. EULDPH: A new technique for making computer-assisted depth estimates from magnetic data. *Geophysics* **47**, 31–37.

Ugalde H.A. and Morris W.A. 2010. Cluster analysis of Euler deconvolution solutions; New filtering techniques and geologic strike determination. *Geophysics* **75**, 61–70.

Venkateswarlu N.B. and Raju P.S.V.S.K. 1992. Fast isodata clustering algorithms. *Pattern Recognition* **25** (3), 335–342.

Vigneresse J.L. 1988. La fracturation post-hercynienne du Massif armoricain d'après les données géophysiques. *Géologie de la France* **4**, 3–10.

Weber C. 1968. Données géophysiques sur le prolongement du socle cristallin du Morvan sous ses bordures sédimentaires. *Bulletin de la Société Géologique de France* **10**(3), 263–272.

Weber C. 1971. Le socle antépermien sous la bordure sud du bassin de Paris d'après les données géophysiques. *Bulletin BRGM, section I* **3**, 177–189.

Weber C. 1973. Le socle antétriasique de la partie sud du bassin de Paris d'après les données géophysiques. *Bulletin BRGM, section II* **3,4**, 219–343.

Weber C. and Lorne J. 1966. Le socle anté-permien dans la bordure sud-ouest du Bassin Parisien. Essai d'interprétation par les méthodes géophysiques. *Bulletin BRGM* **1966–1**, 67–85.

Werner S. 1953. Interpretation of magnetic anomalies at sheet-like bodies. *Sveriges Geologiska Undersokning*, Ser. C **43**, N06.

Yang Y., Li Y. and Liu T. 2010. Continuous wavelet transform, theoretical aspects and application to aeromagnetic data at the Huanghua Depression, Dagang Oilfield, China. *Geophysical Prospecting* **58**, 669–684.